Universality of the Fundamental Diagram in Pedestrian Dynamics

A study based on social force models

Author: Miguel Trigo López

Supervisor: José Ramasco Sukia

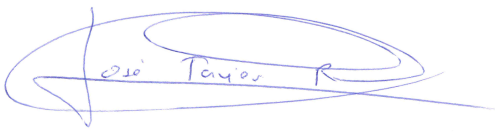

A thesis presented for the master of Complex Systems

Universitat de les Illes Balears
Spain
September 2017

Abstract

The so-called *fundamental diagram* has been a constant in the study of pedestrian dynamics from its origins to the present day. Yet, there is no consensus about the particular form of this function and not sufficient evidence for it to display universality. In this work, a study of the fundamental diagram in different pedestrian facility sets by means of social force models is carried out. Results suggest the fundamental diagram predicted by the social force models used cannot be considered fundamental or universal since its functional shape crucially depends on the geometry of the facility.

Acknowledgments

I would like to express my gratitude to José Ramasco for his guidance, help, availability and friendly treatment during the term of this work. Thanks to my mastermates and my parents, for giving me the opportunity to attend this master.

Contents

1 Introduction **1**

2 Methods **3**
2.1 Social Force Model (SFM) 3
2.1.1 Impatience in counterflows 5
2.2 Anisotropic Social Force Model (ASFM) 6
2.3 A Modified Social Force Model (MSFM) 7
2.4 A Centrifugal-Inspired Social Force Model (CSFM) 8
2.5 Numerical implementation 10

3 Results **13**
3.1 Social Force Model (SFM) test 13
3.2 Fundamental diagram 16
3.2.1 Straight corridor 18
3.2.2 Funneled corridor 21
3.2.3 Rectangle 22
3.2.4 Racetrack 24
3.2.5 Circle 26
3.2.6 Bidirectional corridor 28
3.2.7 Corridor intersection 29

4 Conclusions and future work **33**

1 Introduction

On 24 September 2015, a panic stampede took the life of at least 2.070 people during the annual Hajj pilgrimage in Mina, Mecca, Saudi Arabia [1]. This event added to the growing record of catastrophes induced by crowd motion [2]. Now, more than ever, these incidents are raising awareness in the scientific community regarding the importance of understanding pedestrian dynamics.

The origins of the study of pedestrian dynamics can be traced back to the 1950s when the first empirical observations were made [3]. A series of models were built during the years that followed in an attempt to capture the features of these flows. Depending on their approach, these models can be grouped in several categories [4]. However, in general terms, two types are distinguished: the macroscopic and the microscopic descriptions. Macroscopic modelling is used when a large number of individuals is considered and the focus is set on variables such as pressure or velocity. On the other hand, a microscopic modelling is focused on individuals and the interaction among them. It allows to deal with lower number of pedestrians including particular information of every pedestrian.

The Social Force Model is the most popular in the frame of microscopic modelling. After a thorough study of pedestrian flows in analogy to fluids [5], Helbing and his colleges proposed in 1995 a force model that could reproduce spatiotemporal patterns shown in pedestrian groups under normal conditions with simple interactions rules for the individuals [6]. In contrast to fluid dynamics, this agent-based approach does not require to have into account energy or momentum conservation. The only constraint is mass conservation, introducing thus a great modelling flexibility. In the year 2000 the model was introduced for tackling panic escaping situations reproducing many of the self organized patterns of the former model as well as some of panic escaping situations [7]. These models have been carefully calibrated in several occasions [8, 9].

Over the coming years a great number of modifications have been proposed. However, their calibration with real data is rare. On the whole, these modifications are subtle and do not change the original social force concept. The Social Force Model assumes pedestrians behaviour under normal conditions is, for the most part, predictable. Humans would have developed an automatic response to standard situations. Recent studies on game theory and evolutionary algorithms seem to support this idea [10, 11]. The model describes pedestrian dynamics by means of a series of newtonian forces of physical as well as psychological nature. The velocity and position of a pedestrian is updated after computing the net force acting on each agent, as the sum of all the forces involved.

The Social Force Model can be used to quantify the performance of facilities and shed light on possible improvements in the infrastructure or evacuation protocols [12, 13]. This is the reason why many professionals such as safety and risk managers, architects, urban designers, robotic engineers and transport managers among others are interested in the outcome of these studies. Of particular importance along these lines is the characterization of the so-called *fundamental diagram*, which informs about the capacity of pedestrian facilities.

The fundamental diagram establishes the relationship between velocity v (or flow $\Phi = \rho \cdot v$)

and density ρ of pedestrians and has been a constant in the study of pedestrian dynamics from its origins to the present day [3, 14, 15, 16]. Apart from the expected inverse relationship between density and velocity, there is still no consensus about the particular form of this function. Furthermore, the *fundamental* property is called to question. Information collected by different researchers during the years show considerable disagreement suggesting no universality [17, 18]. Several factors have been proposed as an explanation of these discrepancies including ethnic differences [19, 20], the presence of bidirectional flows [21], the influence of the psychological state of the pedestrians [22] and the measurement technique used [23]. The experimental database of the fundamental diagram is large. However, its comparison with predictions provided by social force models is more difficult to find. Nevertheless, some studies with this purpose have been published lately [24, 25, 26].

Outlook

This work is aimed at performing a systematic test on the fundamental diagram with a series of social force models in different pedestrian sets in order to discuss its form and universality.

2 Methods

This section is aimed at describing the models used in the study of the fundamental diagram and providing the reader with a brief description of the computational implementation of them.

2.1 Social Force Model (SFM)

In the year 2000, Dirk Helbing, Illés Farkas and Tamás Vicsek published a modified version of the original social force model to adapt it to panic escaping situations, in which greater densities are attained [7]. The basic elements of the model consists of pedestrians and walls or obstacles. Each of the N pedestrians i is treated as a circle of radius r_i and mass m_i that heads towards a target and, meanwhile, can interact with walls W and other pedestrians j by means of Newtonian forces.
Three kind of forces are considered.

1. A driving force $\mathbf{f}_0$ that steers pedestrians to their target and makes them adjust to a velocity in which they feel comfortable.

2. Interaction forces among individuals $\mathbf{f}_{ij}$.

3. Interaction forces with obstacles and walls $\mathbf{f}_{iW}$.

The equation of motion of each pedestrian i can be expressed as the sum of these contributions:

$$m_i \frac{\mathrm{d}\mathbf{v}_\mathrm{i}}{\mathrm{dt}} = \mathbf{f}_0 + \sum_{j \neq i} \mathbf{f}_{ij} + \sum_W \mathbf{f}_{iW}. \tag{1}$$

The driving force $\mathbf{f}_0$ takes the form

$$\mathbf{f}_0 = m_i \frac{v_i^0(t)\mathbf{e}_i^0(t) - \mathbf{v}_i(t)}{\tau_i}. \tag{2}$$

Each individual, with coordinates $\mathbf{r_i}$, likes moving with a certain desired velocity v_i^0 along the direction $\mathbf{e}_i^0$ towards the position of the target $\mathbf{r}_t$, where $\mathbf{e}_i^0 = (\mathbf{r}_t - \mathbf{r}_i)/||\mathbf{r}_t - \mathbf{r}_i||$. When this velocity is exceeded, the individual recovers the desired velocity and direction of motion in the characteristic time τ_i. This time accounts for the reaction time of humans plus their acceleration time.

The interaction force among pedestrians $\mathbf{f}_{ij}$ consist of three terms as follows:

$$\mathbf{f}_{ij} = [A_i\, e^{\frac{r_{ij}-d_{ij}}{B_i}} + kg(r_{ij} - d_{ij})]\mathbf{n}_{ij} + \kappa g(r_{ij} - d_{ij})\Delta v_{ji}^t \mathbf{t}_{ij}, \tag{3}$$

where A_i, B_i, k and κ are constants that set the importance of each of the terms involved. The $g(x)$ function is $g(x) = x$ if $x > 0$ and $g(x) = 0$ otherwise. $r_{ij} = r_i + r_j$ is the sum of the radii of individuals i and j, and $d_{ij} = ||\mathbf{r}_i - \mathbf{r}_j||$ denotes the distance between the pedestrians' centers of mass. The vector $\mathbf{n}_{ij} = (n_{ij}^1, n_{ij}^2) = ((\mathbf{r}_i - \mathbf{r}_j)/d_{ij})$ is the normalized vector pointing from the element j to i, while $\mathbf{t}_{ij} = (-n_{ij}^2, n_{ij}^1)$ is the tangential vector perpendicular to $\mathbf{n}_{ij}$. $\Delta v_{ji}^t = (\mathbf{v}_j - \mathbf{v}_i)\mathbf{t}_{ij}$ is the tangential velocity difference.

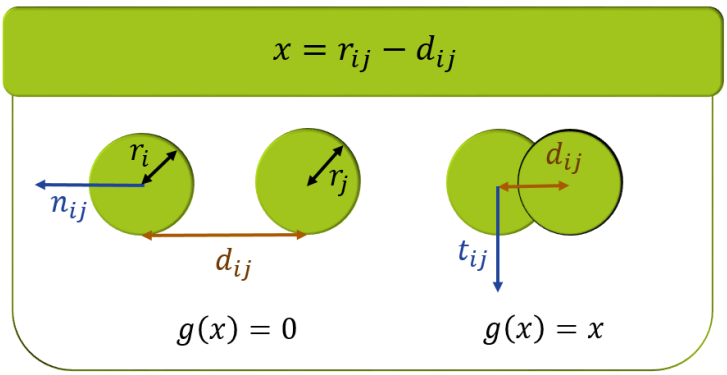

Figure 1: Two situations are depicted. In the left case $r_{ij} < d_{ij}$, then $g(x) = 0$ and the interaction force takes the form $\mathbf{f}_{ij} = A_i \, e^{\frac{r_{ij}-d_{ij}}{B_i}} \mathbf{n_{ij}}$. On the contrary, in the overlapping case $r_{ij} > d_{ij}$, thus $g(x) = x$ and then all of the force terms apply.

All of the terms involved in eq.3 depend on the factor $r_{ij} - d_{ij}$. The sign of this factor indicates if pedestrians radii are overlapping or, on the other hand, they are separated. The specific value informs about the extent to which the previous situations take place. When pedestrians do not overlap, $g(r_{ij} - d_{ij}) = 0$ and then, only the term $A_i \, e^{\frac{r_{ij}-d_{ij}}{B_i}} \cdot \mathbf{n}_{ij}$ applies. The first two terms of eq.3 are applied in the direction that joins the pedestrians' center of mass $\mathbf{n}_{ij}$ and describe the repulsive tendency to separate from each other. The first term $A_i \, e^{\frac{r_{ij}-d_{ij}}{B_i}} \cdot \mathbf{n}_{ij}$ shows an exponential dependence on the distance between pedestrians. This term decays to zero as pedestrians set apart and it is inspired by the psychological tendency to be separated from others. The two remaining terms are inspired by granular media interactions. The second term $kg(r_{ij} - d_{ij}) \cdot \mathbf{n}_{ij}$ is the *body force*. Note it is a spring-like force of elastic constant k. It decays linearly as pedestrians separate. The effect of this term is to assist the first term in counteracting body compression when pedestrians interact physically. The third term $\kappa g(r_{ij} - d_{ij}) \Delta v^t_{ji}$ is the *sliding friction force* and describes how difficult is tangential motion when pedestrians are overlapping. This force depends linearly on the centers of mass separation and relative tangential velocity difference.

The interaction each pedestrian i experiences with the walls W takes the form

$$\mathbf{f}_{iW} = [A_i e^{\frac{r_i - d_{iW}}{B_i}} + kg(r_i - d_{iW})]\mathbf{n}_{iW} - \kappa g(r_i - d_{iW})(\mathbf{v}_i \mathbf{t}_{iW})\mathbf{t}_{iW}. \tag{4}$$

A first glance at eq.4 lets us know interaction with walls are treated analogously to other pedestrians. However, some differences must be commented. Instead of circles with a characteristic radius and velocity, walls are modeled as point-like static sources. Thus, only the radius and velocity of pedestrians appear in the previous equation. The *sliding friction force* term carries a minus sign instead of the plus sign written in eq.3. This is just a direct result of the walls having null velocity.

The Social Force Model (SFM) was calibrated to reproduce the distance kept at normal desired velocities and fit the measured flows through bottlenecks for 1 meter wide doors when $v_i^0 = 0.8$ ms^{-1}. The estimation for the parameters is $A_i = 2000$ N, $\tau_i = 0.5$ s,

$B_i = 0.08$ m, $k = 1.2 \cdot 10^5$ Kg s^{-2}, $\kappa = 2.4 \cdot 10^5$ Kg m^{-1} s^{-1} when $m = 80$ Kg and $2 \cdot r_i \in [0.5 \text{ m}, 0.7 \text{ m}]$. In reality, each pedestrian should have a different specification of the parameters. However, for reasons of simplicity, they were set constant and equal to all the agents. Only the radius was given certain freedom in order to avoid permanent gridlocks at exits.

Two extra modifications based on the original form of the model of 1995 [6] can be introduced in the dynamics. These are a maximum possible velocity and a force term accounting for fluctuations. Note that no limits in the pedestrians' velocity are provided by the Social Force Model (SFM). If two pedestrians place themselves close enough their velocity can tend to infinity. This situation is seldom found in this model due to the contact forces. In its original form this scenario was more probable and it was tackled by setting a maximum achievable velocity. Since high densities are expected to be attained for the purpose of this work, a maximum achievable velocity was set to ensure normal behavior. The actual velocity $\mathbf{v}_i$ is a function of the preferred velocity $\mathbf{w}_i$ and depends on a maximum velocity v_{max}.

$$\frac{d\mathbf{r}_i}{dt} = \mathbf{v}_i := \mathbf{w}_i \cdot g(\frac{v_{max}}{||\mathbf{w}_i||}) \tag{5}$$

where

$$g(\frac{v_{max}}{||\mathbf{w}_i||}) = \begin{cases} 1 & \text{if } ||\mathbf{w}_i|| \leq v_{max} \\ \frac{v_{max}}{||\mathbf{w}_i||} & \text{Otherwise} \end{cases}$$

This tells us that if the modulus of the velocity of a pedestrian derived from computing the net force acting on it exceeds the maximum velocity, the actual velocity will conserve the ratio between components but the modulus will equal the maximum achievable.

Motion can be benefited from force fluctuations. These allow pedestrians to find new paths when they collide with other walkers or remain stuck at exits. A stochastic force term $\mathbf{f}_\epsilon$ can be introduced in the dynamics leaving them as

$$m_i \frac{\mathrm{d}\mathbf{v}_\mathrm{i}}{\mathrm{dt}} = \mathbf{f}_0 + \sum_{j \neq i} \mathbf{f}_{ij} + \sum_W \mathbf{f}_{iW} + \mathbf{f}_\epsilon. \tag{6}$$

2.1.1 Impatience in counterflows

Counterflows in pedestrians intending to escape can trigger panic situations. Pedestrians become impatient when they are unable to move in the direction of their target for a long time. This translates in constant pushes and attempts to move faster. These effects can be integrated in the model as commented in [7]. A panic parameter fulfilling $0 \leq p_i(t) \leq 1$ can be measured in order to model the extent to which pushes or velocity increments take place. The panic parameter obeys

$$p_i(t) = 1 - \frac{\bar{\mathbf{v}}_i(t)}{v_i^0}, \tag{7}$$

where $\bar{\mathbf{v}}_i(t)$ is the mean velocity in the direction of the target.

A desired speed increment due to impatience can be described in the next manner:

$$v_i^0(t) = [1 - p_i(t)]v_i^0(0) + p_i(t)v_i^{max}, \tag{8}$$

where $v_i^0(0)$ and v_i^{max} are the initial and maximum desired velocities of pedestrian i respectively.

Panic can also trigger an increment in the fluctuations simulating pushes and discontinuous motion. This fluctuation term being a gaussian random variable of zero mean and standard deviation $\eta_i(t)$ dependent on the level of panic analogously to eq.8:

$$\eta_i(t) = [1 - p_i(t)]\eta_i^0(0) + p_i(t)\eta_i^{max}, \tag{9}$$

where $\eta_i^0(0)$ is the minimum and η_i^{max} is the maximum fluctuation strengths.

The panic parameter in eq.7 has been said to lie between 0 and 1, giving then meaning to eq.8 and eq.9. However, eq.7 allows a wider range. Values above 1 and bellow 0 are also permitted since the mean velocity in the desired direction can eventually be greater than the desired velocity, and the mean velocity can carry a minus sign. For this reason, whenever the panic parameter exceeds these boundaries, it is set to the closest limit.

2.2 Anisotropic Social Force Model (ASFM)

Typically pedestrians show a different reaction depending on the angle of encounter ϕ_{ij} among them. This anisotropy can be integrated in the model by adding a multiplying prefactor $w(\phi_{ij}(t))$ to the first force term as shown in [2]. The interaction force term turns into

$$\mathbf{f}_{ij} = [A_i w(\phi_{ij}(t))\ e^{\frac{r_{ij}-d_{ij}}{B_i}} + kg(r_{ij} - d_{ij})]\mathbf{n}_{ij} + \kappa g(r_{ij} - d_{ij})\Delta v_{ji}^t \mathbf{t}_{ij}. \tag{10}$$

The second and third terms are forces of physical nature due to actual collisions, so no anisotropy is included there. The prefactor reads as follows:

$$w(\phi_{ij}(t)) = \lambda_i + (1 - \lambda_i)\frac{1 + cos(\phi_{ij})}{2}, \tag{11}$$

where

$$cos(\phi_{ij}) = \frac{\mathbf{v}_i}{||\mathbf{v}_i||} \cdot \frac{-(\mathbf{r}_i - \mathbf{r}_j)}{d_{ij}} \tag{12}$$

and λ_i is a parameter which lies in the range $0 \leq \lambda_i \leq 1$ and calibrates the strength of encounters from behind. Evolutionary calibration with empirical data suggests $\lambda_i \approx 0.1$ in the original social force model of 1995 [2]. Eq.12 measures how much of the pedestrian i's velocity is pointing towards pedestrian j. When pedestrian i's velocity is pointing to the opposite sense of pedestrian j: $cos(\phi_{ij}) = -1$ and then $w(\phi_{ij}(t)) = \lambda_i$. On the contrary, when pedestrian i's velocity is directly pointing towards pedestrian j: $cos(\phi_{ij}) = 1$ and then $w(\phi_{ij}(t)) = 1$.

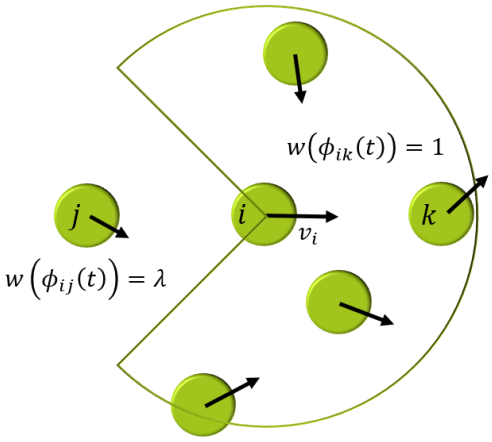

Figure 2: Schematic representation of the two limiting cases for the anisotropic prefactor.

2.3 A Modified Social Force Model (MSFM)

According to Daniel R. Parisi [24] the Social Force Model (SFM) presents large limitations when describing the main macroscopic observables that characterize normal pedestrian flow dynamics: the specific flow rate and the fundamental diagram. Parisi and coworkers mention that this occurs because the Social Force Model (SFM) is always in a competitive state. A first approach to the Social Force Model (SFM) might suggest that the desired velocity v^0 is the behavioral control parameter. By turning this parameter from low to high values, one would change the dynamics of the system from a normal to a panic state. However, they continue arguing that this does not occur. The Social Force Model (SFM) does not prevent slowly pedestrians, such as elderly people, from panicking. A continuous pushing occurs no matter the desired velocity of motion.

The authors propose a self-stopping mechanism to turn the model into a normal flow model in which people slow down before pushing. This is fulfilled by defining a respect radius such that if this region is trespassed by another pedestrian, the desired velocity of the former is immediately set to zero. Note that this does not prevent the pedestrian from moving, since only v^0 is affected. However, according to eq.2 the instantaneous velocity $\mathbf{v}_i(t)$ would eventually drop to zero if the respect radius remains occupied.

Let us define the respect distance of the agent i D_{R_i} as

$$D_{R_i} = R_F \cdot r_i, \tag{13}$$

where R_F is the respect factor, defined as a positive real number, and r_i is the radius of pedestrian i. The respect area is the circle of radius D_{R_i} centered at the point C_i^R along the direction of the desired velocity (see Fig.3). Note that the respect circle always crosses the center of the pedestrian.

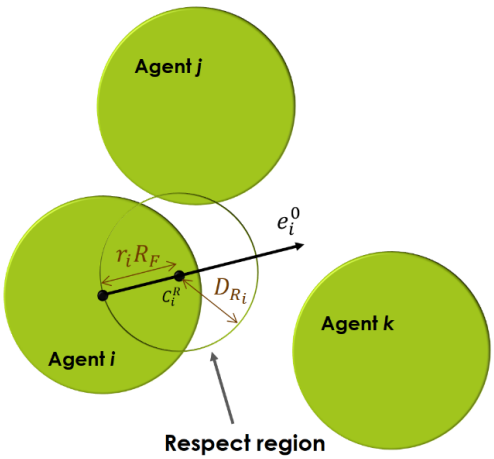

Figure 3: The geometrical aspects of the respect area of particle i are represented. Under the circumstances depicted in the figure, the desired velocity of particle i is $v_i^0 = 0$ since particle j is trespassing particle i's respect region.

In order to calibrate the value of the respect factor R_F, an investigation of the pedestrian escaping rate was effectuated in a square room of 20 m of side for different exit widths and different number of pedestrians. Experimental results from the literature suggest an evacuation rate ranging from 1.25 to 2 p/m/s under normal conditions when the door width changes. A respect factor of $R_F = 0.7$ m reproduced a range of specific flow rates between 1.2 and and 2 p/m/s when the mass, diameter and desired velocity of pedestrians were uniformly distributed within the ranges $m \in [70 \text{ kg}, 90 \text{ kg}]$, $d \in [0.50 \text{ m}, 0.58 \text{ m}]$ and $v_0 \in [0.9 \text{ m/s}, 1.5 \text{ m/s}]$.

2.4 A Centrifugal-Inspired Social Force Model (CSFM)

Typically, pedestrians react differently to an approaching pedestrian depending on the velocity at which the pedestrian is approaching them. When a pedestrian is approached by another at a high velocity he changes its direction to avoid collision, even if the other pedestrian is still far apart. However, no long-range velocity dependent force term is present in the Social Force Model (SFM). This leads to unrealistic behaviours in counterflows. In this work a long-range force term dependent on the relative velocity among pedestrians is added to the Social Force Model (SFM) to investigate the differences encountered in the fundamental diagram. This term takes the next form

$$\mathbf{f}_{ij}^C = C_i m_i w(\phi_{ij}(t)) \frac{v_{ij}^2}{d_{ij}} \mathbf{n}_{ij}, \tag{14}$$

where C_i is a constant that weights the interaction. For simplicity $C_i = 1$ although it requires proper calibration. v_{ij} is given by

$$v_{ij} = \frac{1}{2}[\ (\mathbf{v}_j - \mathbf{v}_i)\mathbf{n}_{ij} + ||(\mathbf{v}_j - \mathbf{v}_i)\mathbf{n}_{ij}||\ ].$$

Two possible cases are distinguished for v_{ij}:

$$v_{ij} = \begin{cases} (\mathbf{v}_j - \mathbf{v}_i)\mathbf{n}_{ij} & \text{if } (\mathbf{v}_j - \mathbf{v}_i)\mathbf{n}_{ij} > 0 \\ 0 & \text{Otherwise.} \end{cases}$$

This tells us that, if pedestrians are not approaching, the term v_{ij} vanishes. The dynamics of the system are described by

$$m_i \frac{\mathrm{d}\mathbf{v}_\mathrm{i}}{\mathrm{dt}} = \mathbf{f}_0 + \sum_{j \neq i} (\mathbf{f}_{ij} + \mathbf{f}_{ij}^C) + \sum_W \mathbf{f}_{iW} + \mathbf{f}_\epsilon.$$

The new term of eq.14 is based on the Centrifugal Force Model [27]. However, some differences between both implementations are worth commenting. In our study the term $\mathbf{f}_{ij}^C$ gives some credit to pedestrians approaching from the back in contrast to the Centrifugal Force Model. In the original model no distance dependent force is combined with the velocity dependent force. Thus, if two pedestrians happen to move at the same velocity with almost no separation between them they will continue their motion together without any interaction at all. Here the psychological tendency to be separated is added according to the SFM scheme. In the Centrifugal Force Model an algorithmic mechanism is implemented to avoid overlaps. Instead, we include the contact forces of the SFM to prevent great overlaps, although they remain possible to some extent.

2.5 Numerical implementation

The Social Force Model (SFM) and some modifications have been introduced in the previous section. Numerical implementations are key to understand their performance. In this section the numerical approach taken in this work is presented. Pseudocode 1 shows the basic structure of a program aimed to simulate the motion of pedestrians ruled by the Social Force Model (SFM).

Algorithm 1 SFM pseudocode

```
1:  Initialize Pedestrians and Walls
2:  for all TimeStep do
3:      for all Pedestrian i do
4:          F_ij = 0
5:          F_iW = 0
6:          for all Pedestrian j ≠ i do
7:              Calculate f_ij                    ▷ Force effectuated by pedestrian j on i
8:              F_ij = F_ij + f_ij                ▷ Storage of all pedestrian forces on i
9:          for all Wall W do
10:             Calculate f_iW                    ▷ Force effectuated by wall W on i
11:             F_iW = F_iW + f_iW                ▷ Storage of all wall forces on i
12:         Calculate f_0 and f_ϵ                 ▷ Steering force and fluctuations of pedestrian i
13:         F_i = f_0 + F_ij + F_iW + f_ϵ         ▷ Force on i is the sum
14:         Update i's velocity
15:         Update i's position
```

In *line 1* pedestrians and walls are initialized. Pedestrians are given a radius, mass, desired velocity and initial location. Walls, in turn, are only given static and discrete locations. Pedestrians must be initialized within the limits of the facilities. A rejection method is used for this purpose. Pedestrians were first given random coordinates in a larger area. When the position provided lied outside the desired limits or it was closer than $d_{ij} = 0.35$ m from other pedestrians it was rejected and new random coordinates were proposed. The process was repeated until acceptance was reached.

Every time step (*line 2*), the net force acting on each pedestrian is independently computed for the two coordinates of motion. In *line 3* pedestrian i is selected. The force f_{ij} is computed for every pair of pedestrians ij, $i \neq j$ by means of eq.3 and the summation is stored (*lines 6-8*). Then, the same process is effectuated with the discrete point like walls (*lines 9-11*). The interaction force with non overlapping pedestrians and walls decays exponentially with the distance leading to negligible values rapidly. Therefore, in order to save computational time, the interaction was restricted to the closest elements. Only pedestrians and walls lying within a radius of 3 m from the pedestrian evaluated where taken into account. In the CSFM the maximum distance at which the force is computed is set in $d^C = 2$ m. In this case, higher values for d^C can lead to different dynamics since the velocity-dependent force term does not decay as fast as the SFM term. Eventually, the steering force term is calculated in *line 12* by means of eq.2. In order to do this, the

steering normalized vector e_i^0 is first updated. When pedestrians were supposed to take drifts to follow different directions in the facility, different targets were defined. The target of each pedestrian was set depending on their position in the facility. The net force is then calculated in *line 13* for each dimension independently. The system of second order coupled equations is solved to update the velocity and position of pedestrian i. The Milshtein algorithm is used to update the velocity in case fluctuations are included. The Euler scheme is used to update the position of the walkers. Despite its error $O(h^2)$, the Euler method is highly used in the social force community. Under the presence of additive noise, the Milshtein algorithm turns into the Euler-Maruyama algorithm. Then, the velocity update is effectuated as

$$v(t+h) = v(t) + \frac{h}{m}(f_0 + F_{ij} + F_{iW}) + \frac{\sqrt{\sigma^2(f_\epsilon)\cdot h}}{m}\hat{u_\epsilon} + O(h^{3/2}),$$

where $\hat{u_\epsilon}$ is a gaussian random variable of zero mean and variance 1, and $\sigma^2(f_\epsilon)$ is the variance of the noise term f_ϵ. Then, the position update is effectuated within an Euler scheme:

$$x(t+h) = x(t) + v(t+h)h + O(h^2).$$

When the updated velocity was greater than the maximum achievable, it was modified by means of eq.5. Then, the pedestrian's position was updated. Under high pressure conditions, pedestrians can actually penetrate walls. In order to avoid this, a numerical restriction can be imposed. Whenever the updated position of pedestrian i means passing through a wall, the position of the pedestrian is placed in the limits of the wall, a distance $d_{iW} = 0.05$ m. If the time step used is sufficiently small, this process is not abrupt.

In order to implement the Modified Social Force Model (MSFM), another circle is initialized in *line 1*. It has the radius D_{R_i} specified in eq.13 placed along the desired direction of motion crossing the pedestrian's center of mass. In the loop defined in *line 6* the distance between the center of mass of pedestrian i's respect area and pedestrian j's center of mass is computed. When, for any of the pairs ij, this distance is less than the sum of the radii involved the respect area is occupied. Then, if it is occupied, the steering force is calculated by setting the desired velocity to zero in *line 12* . Otherwise, the steering force is calculated as usual. The respect area is updated every time the desired direction of motion is updated.

Sometimes, periodic boundary conditions are implemented in the simulations. Whenever the pedestrian's location reached the exit of the facility, it was placed again nearby the entrance. The distance from the entrance being the same as the distance the previous movement separated it from the exit. Pedestrians in the surroundings of the facility limits have to interact with the pedestrians of the other limits as if they were next to them. In order to make this possible, pedestrians j in *line 6* were sometimes assigned new and temporal coordinates during the force calculation process. This was effectuated by temporally applying the periodic boundary conditions commented above. Fig.4 shows a scheme of the process in a straight corridor. Note 5 different cages are depicted. Due to the explained procedure, pedestrians in one of the cages only consider pedestrians located in their cage and the two immediate neighbour cages. The same exact process was effectuated with the walls.

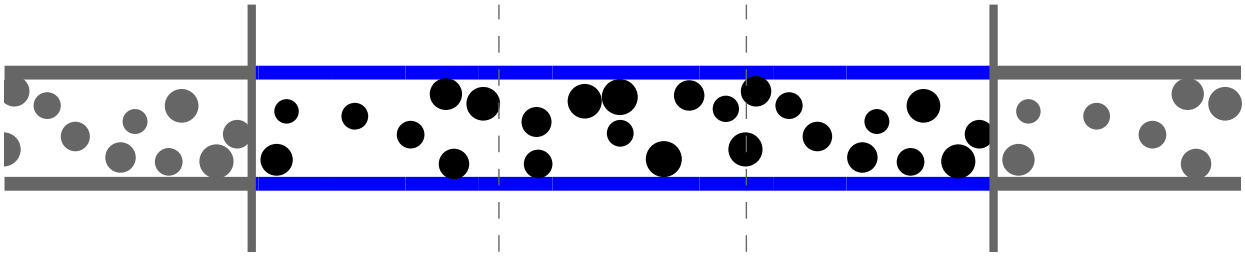

Figure 4: Periodic boundary conditions in a straight corridor. The corridor in blue and pedestrians in black are the real elements of the system. Pedestrians in grey are an extension of the real pedestrians of the opposite side of the real corridor.

3 Results

This section is organized in two parts. The first part is aimed at testing the implementation of the Social Force Model as well as showing relevant phenomena in pedestrian dynamics. The second part is devoted to the fundamental diagram in different geometries.

3.1 Social Force Model (SFM) test

In order to check the Social Force Model implementation, several self-organizing phenomena were successfully reproduced. These were: *transition to incoordination due to clogging*, the *faster is slower* effect, *lane formation* and *oscillations at exits*. The dynamics of the Social Force Model implemented in this section is given by eq.1, being the forces described by eq.2, eq.3 and eq.4. Note that no noise or maximum achievable velocity were considered.

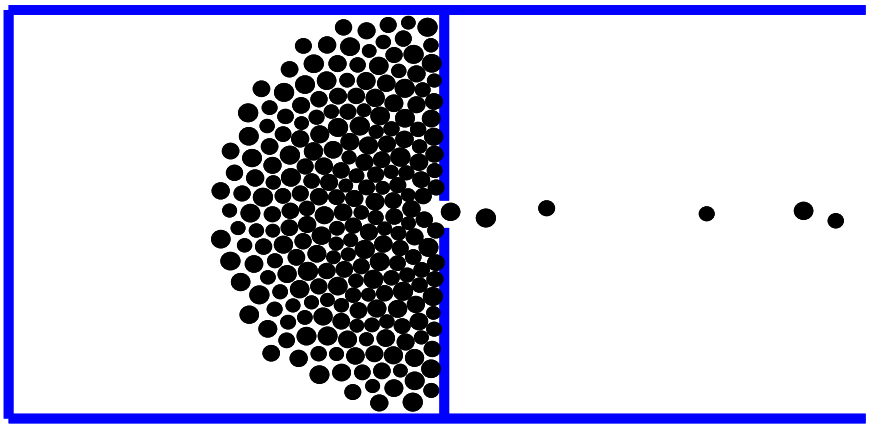

Figure 5: Pedestrians in a squared room of 15 meters of side that head towards a 1 m width door at an equal desired speed $v^0 = 3.5$ ms^{-1}. Agent's mass and diameter were $m = 80$ Kg and $2 \cdot r_i \in [0.5\text{ m}, 0.7\text{ m}]$.

Fig.5 shows a simulation of pedestrians in a room that try to exit through a 1 m exit at the desired velocity $v^0 = 3.5$ m/s. After having exited, pedestrians were given a constant and equal velocity, and were left insensitive to further interactions. Thus, the distance among pedestrians after their exit indicates intermittent escaping times. The time required for $N = 200$ pedestrians to leave the room was investigated as a function of the desired speed in Fig.6a. 10 runs were used for each measurement. In general terms three regimes are observed. For normal walking $v^0 < 1.5$ m/s the escaping time decreases as v^0 increases. For $v^0 > 1.5$ m/s the evacuation time decreases with growing v^0. When a group of pedestrians try to move faster, the overall escaping time is greater than when they try to move slower. This effect is known as the *faster is slower effect* and is here predicted. A constant evacuation time could appear for $v^0 \gtrapprox 7$ m/s. However, this range of velocities does not represent pedestrian dynamics and yet greater desired velocities should be measured to ensure the presence of this constant rate.

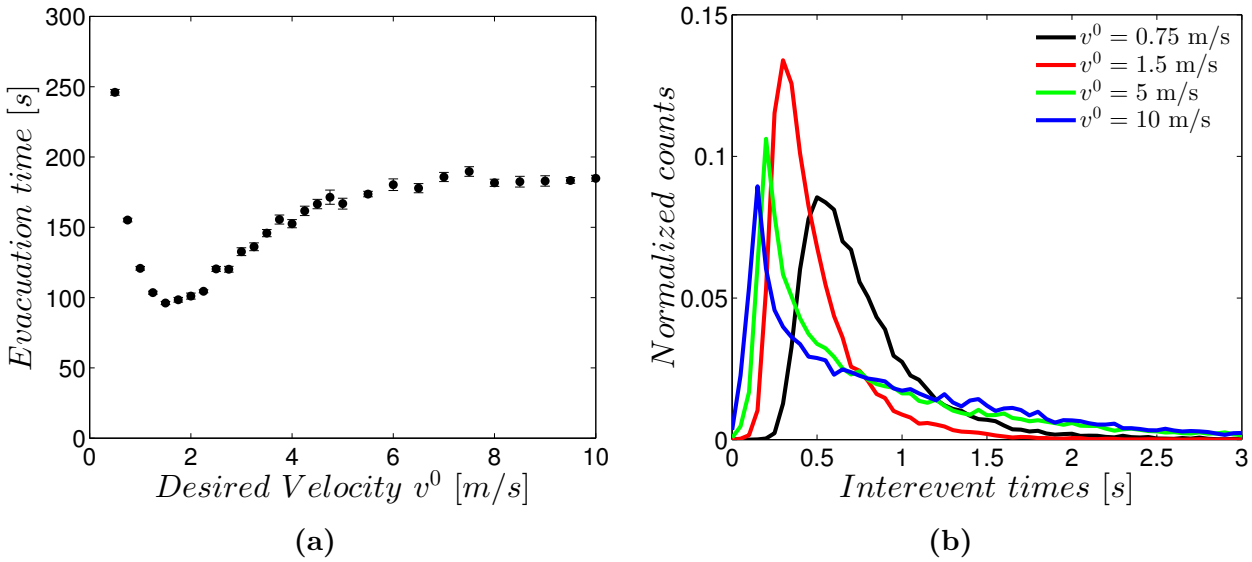

Figure 6: a) Evacuation time of 200 people as a function of the desired velocity when there were initially 250 pedestrians inside the room shown in fig.5. b) Histogram of the time between exits as a function of the desired velocity.

The initial number of pedestrians in the room was $N = 250$, although the number of pedestrians studied was $N = 200$. This extra number of pedestrians was required to avoid permanent gridlocks. When the desired velocities are low, there is a small number of pedestrians, or both situations simultaneously present, the steering force plus the interaction force experienced by the individuals from behind is unable to overcome the repulsive forces of the walls in the surroundings of the exit. This situation is not commented in [7] and suggests that the actual evacuation time predicted by the model depends on the number of pedestrians in the room. This dependency might be subtle at great velocities, but it is infinitely large at low velocities.

Fig. 6b shows a normalized histogram of the time between individual exits as a function of the desired velocity. 100 runs were used for each velocity. Fig.6b in combination with Fig.5 describe the self-organized phenomenon of *Transition to incoordination due to clogging*. Pedestrians outflow is regular and coordinated bellow $v^0 < 1.5$ m/s, but as the velocity increases the outflow turns irregular and avalanche-like due to the breaking of arch-like blockings at the exit.

Despite having been introduced to deal with panic escaping situations, the Social Force Model (SFM) is also able to reproduce self-organizing phenomena also observed under normal conditions. Some examples are *oscillations at exits* and *lane formation*.

The effect of oscillations at exits is depicted in Fig.7. It shows the case for oppositely heading groups that steer to a 1 m exit. Jamming occurs at the doorway. However, when a pedestrian is able to pass, it is easily followed by other pedestrians with the same desired walking direction while the opposed headed group has to wait. When a gap is found in the doorway it is rapidly used by pedestrians heading in the opposite direction. In order to observe this effect under the conditions shown in Fig.7, pedestrians were given a wider range

of possibilities for their radii, being $r_i \in [0.15\text{ m}, 0.35\text{ m}]$.

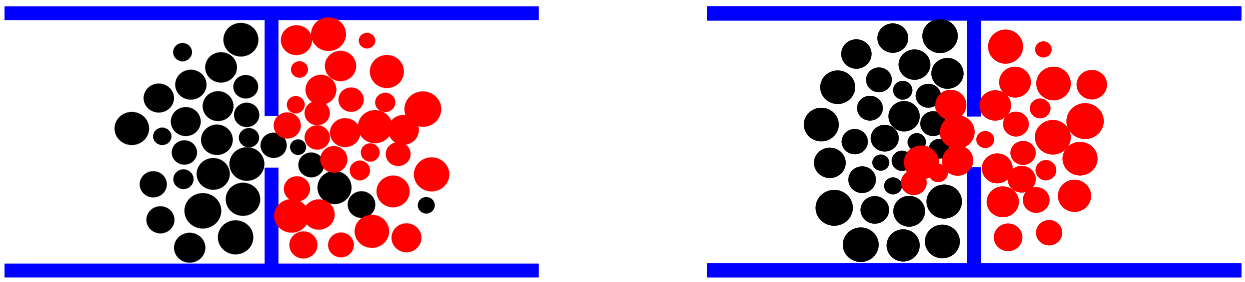

Figure 7: Crossing oscillations in a 1 m door observed when two opposed heading groups coincide. Pedestrians' velocity and mass are $v^0 = 3.5$ m/s and $m = 80$ Kg. Their radii are uniformly distributed in the range $r_i \in [0.15\text{ m}, 0.35\text{ m}]$.

Fig.8 shows the *lane formation* phenomenon. Oppositely heading groups were randomly initialized in between the two walls of the corridor. After a transient time, lanes are formed. The number of lanes depends linearly on the width of the corridor [6]. If no noise is added, a final configuration of lanes remain forever. The presence of large-enough noises or high pedestrian densities can break lanes. Lane formation minimizes unwanted interactions with other pedestrians, therefore, maximizing flow. This pattern has been viewed as an example of a collective intelligent behaviour ruled by simple interaction rules.

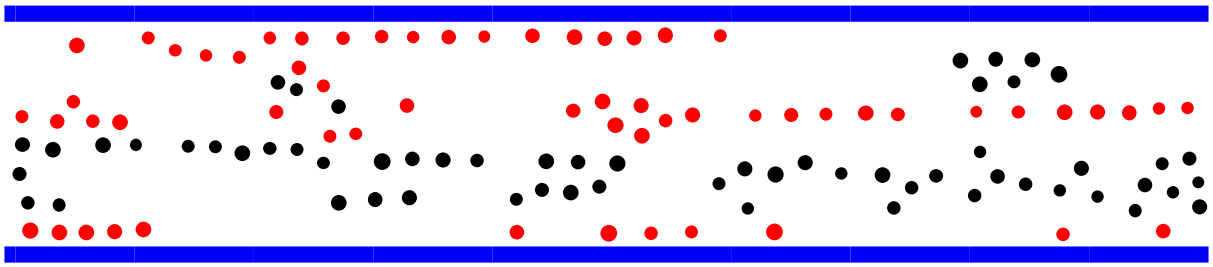

Figure 8: Red and black circles are headed in opposite senses in a corridor of 10 meters width and 50 meters long with periodic boundary conditions at constant desired velocity $v^0 = 1.5$ m/s. Lane formation is observed above a critical density value.

3.2 Fundamental diagram

Typically, in an empirical investigation, the density of pedestrians in the facilities is controlled by setting entrances and exit doors to the facility of variable width for a constant number of pedestrians. Then, a measurement region is defined in which the density and velocity of pedestrians is assessed. The measurements are taken in a stationary regime of density and velocity, avoiding the beginning as well as the last moments of the experiment. However, in a simulation study a slightly different approach might provide greater benefits. The facilities are set periodic when possible in order to avoid dealing with an ending transient. According to [24] the escaping flow rates predicted by the Social Force Model (SFM) for different door widths do not agree with the empirical data. Thus, difficulties to obtain the desired densities may arise from simulating entrances and exit doors. For this reason, the density of pedestrians is controlled by placing different number of pedestrians in the facility directly. The number of pedestrians required to have a density of 4 m^{-2} in the facility is calculated. Then, this number of pedestrians is divided in 14 uniformly distributed numbers. 14 different simulations are carried out with each of this number of pedestrians.

The parameters used in the simulations that follow are presented in tab.1

Parameters	Values	Parameters	Values
m	[70 90] Kg	$2 \cdot r_i$	[0.5 0.58] m
τ_i	0.5 s	R_F	0.7
A_i	2000 N	v_{max}	9 ms^{-1}
B_i	0.08 m	$\sigma^2(f_\epsilon)$	25
k	$1.2 \cdot 10^5$ Kgs^{-2}	λ	0.1
κ	$2.4 \cdot 10^5$ $\mathrm{Kgm}^{-1}\mathrm{s}^{-1}$	d^C	2 m
v^0	[1.1 1.5] ms^{-1}	h	0.001 s

Table 1: Parameters used in the different models for the study of the fundamental diagram

Individuals are headed to the nearest point of the target locations at least 0.2 m separated from the walls in order to avoid unrealistic steerings. The discretization of the walls is effectuated every 0.2 m. When k pedestrians are present in the measurement region, the velocity measured is the mean component of the velocity pointing to the next target. This is

$$\langle v \rangle = \frac{1}{k} \sum_{i=1}^{k} \mathbf{v_i}(t) \cdot \mathbf{e}_i^0(t).$$

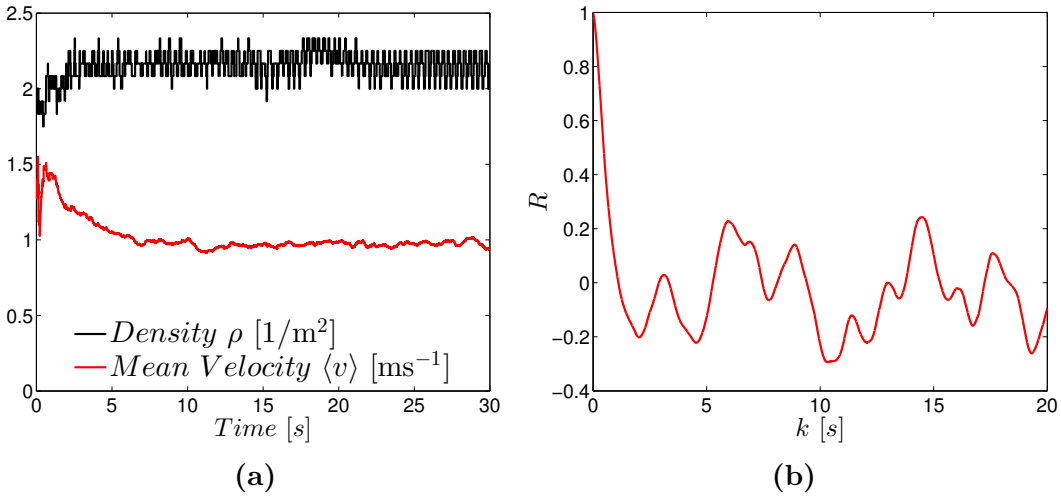

Figure 9: a) Time series of density and velocity for a funneled corridor of $l_c = 20$ m when $N = 141$ pedestrians were present. b) Autocorrelation estimation of the mean velocity in the stationary regime.

Fig.9a shows the density and mean velocity time series within the limits of the measurement region of $l_c = 20$ m in the funneled corridor (see fig.14) when $N = 141$ pedestrians are initialized. An initial transient can be noted up to the first $t_{trans} \approx 10$ s of simulation. Fig.9b presents an estimation of the autocorrelation R according to eq.15 for the mean velocity time series in the stationary regime.

In a discrete process of n measurements $v_{i=1,\dots,n}$, mean velocity $\bar{v}$ and variance σ^2, the autocorrelation at a time distance k can be estimated by the next expression:

$$R(k) = \frac{1}{(n-k)\sigma^2} \sum_{t=1}^{n-k} (v_t - \bar{v})(v_{t+k} - \bar{v}). \tag{15}$$

Correlation is rapidly lost around the first second $t_{cor} = 1$ s. The time series of the other scenarios treated present the same characteristics. For this reason, measurements are taken every second $t_{cor} = 1$ s after the initial transient $t_{trans} = 10$ s .

Simulations run over $t_{mes} = 500$ s for each of the 14 number of pedestrian sets. During this time, measurements lead to a cloud of points in the fundamental diagram. An example is provided in Fig.10. The analysis effectuated consists of averaging over the velocities as long as the density involved is attained more than 10 times. Velocities registered at densities not repeated at least 10 times are rejected.

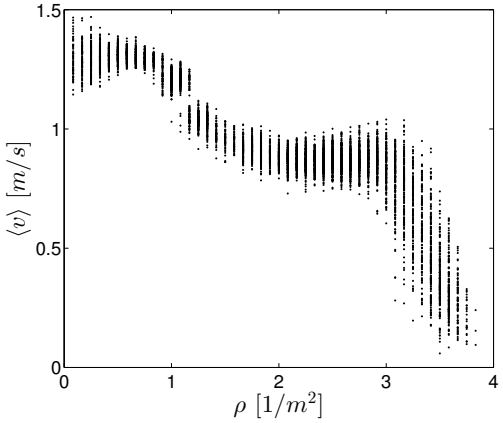

Figure 10: Cloud of measurements given by the Social Force Model (SFM) registered for the fundamental diagram in the funneled corridor with $l_c = 10$ m after a measurement time of $t_{mes} = 500$ s.

Different geometries are presented in this section. First, a description of the parameters that define the facility is made. The Modified Social Force Model (MSFM) is used in the representation of the facilities in order for the reader to know the desired direction of motion at every stage of the structure. Then, the particular aspects of the fundamental diagram study are commented. A chart of four figures follow with the predictions of the models: the Social Force Model (SFM), the Anisotropic Social Force Model (ASFM) with $\lambda = 0.1$, Modified Social Force Model (MSFM) with $R_F = 0.7$ and Centrifugal-Inspired Social Force Model (CSFM) with $d^C = 2$ m and $C_i = 1$. In all cases, noise was introduced according to eq.6. The noise component being a gaussian random variable of zero mean and variance $\sigma^2(f_\epsilon) = 25$.

3.2.1 Straight corridor

The straight corridor is the most simple geometry that can be studied. Fig.11 shows the periodic corridor of width b_{cor} and length l_c used in the simulations. The measurement region is restricted by the distance m_d. Pedestrians' desired direction of motion was the same for all of the individuals. They headed to the right with no perpendicular component $\mathbf{e}_i^0(t) = (1, 0)$.

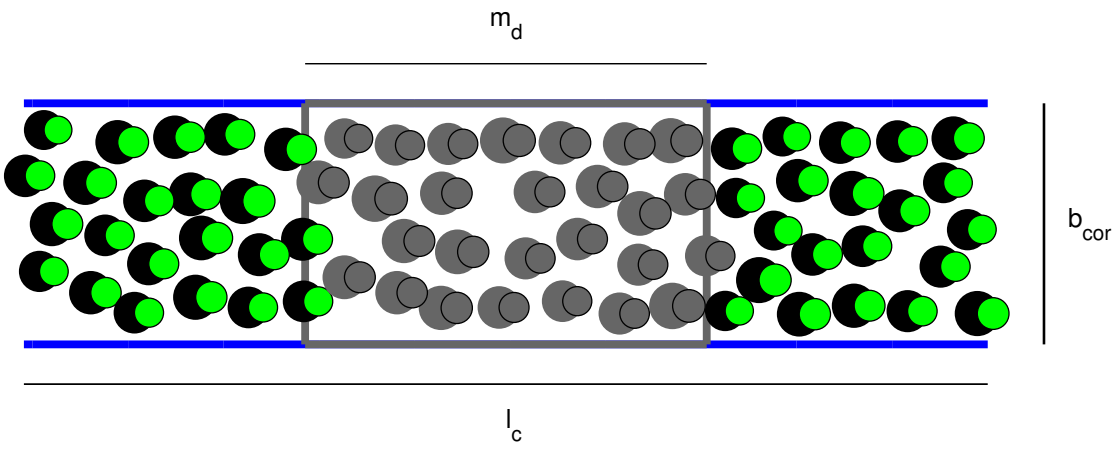

Figure 11: Geometry of the simulated corridor for the measurement of the fundamental diagram. The snapshot corresponds to a simulation with $m_d = 5$ m, $l_c = 12$ m and $b_{cor} = 3$ m.

The fundamental diagram was evaluated as a function of the width of the corridor b_{cor} for a fixed length $l_c = 12$ m in a region delimited by $m_d = 5$ m. The set of widths studied was $b_{cor} = 1, 2, 3, 4, 5$ m. The results of the simulations are registered in Fig.12. Significant differences are found for the smallest width $b_{cor} = 1$ m in comparison with larger widths in the SFM, MSFM and CSFM. The SFM and CSFM do not show apparent differences. These models predict a sudden increase in velocity above the desired velocity around $\rho \approx 3.8$ m^{-2} followed by an abrupt drop to $\langle v \rangle = 0$ m/s for $b_{cor} \geq 2$ m. The MSFM predicts a sooner drop in the fundamental diagram anticipated by a constant velocity regime. This drop is smoother than the one predicted in SFM and CSFM. Two regimes of decay are found in the ASFM predicting a vanishing velocity at $\rho_0 \approx 1.9$ m^{-2}.

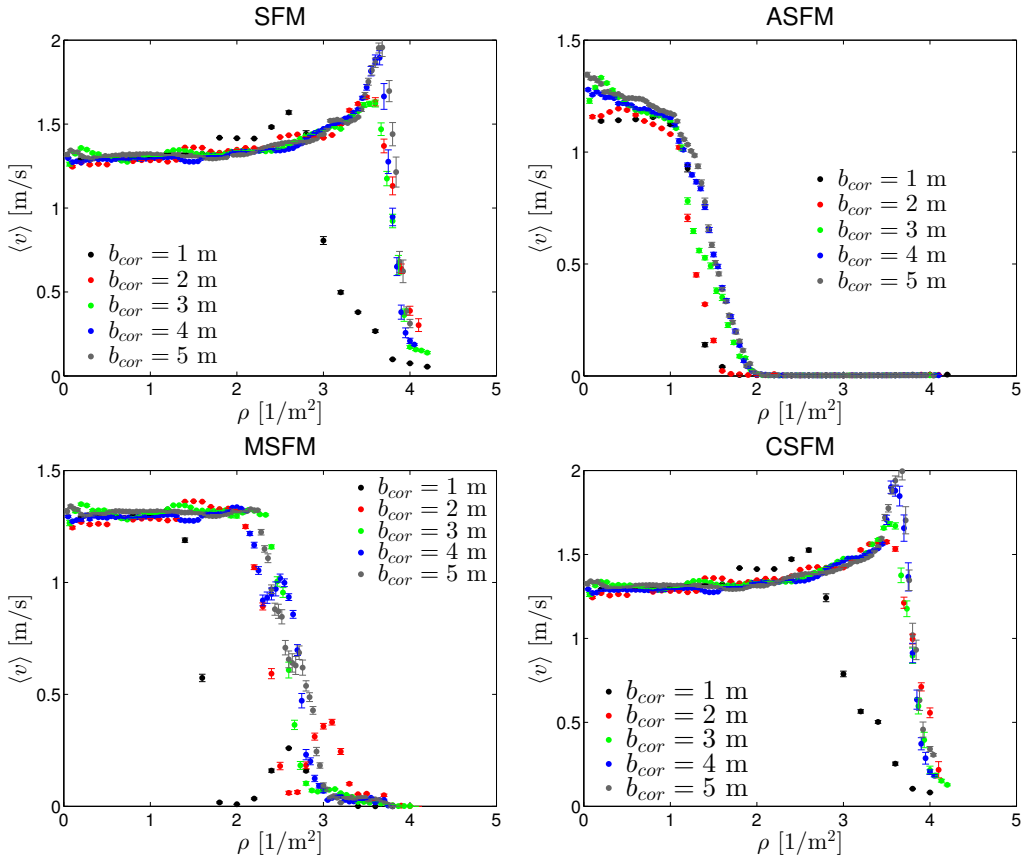

Figure 12: Fundamental diagrams of a straight periodic corridor of $l_c = 12$ m as a function of the width b_{cor}. Social Force Model (SFM), Anisotropic Social Force Model (ASFM), Modified Social Force Model (MSFM), Centrifugal-Inspired Social Force Model (CSFM).

The MSFM for $b_{cor} = 1$ m and $b_{cor} = 2$ m presents a maximum after having reached $\langle v \rangle = 0$ m/s for the first time. This effect is due to the configuration pedestrians achieve depending on their density. Fig. 13 shows the configuration of pedestrians for $b_{cor} = 1$ m when they reach the densities $\rho \approx 2$ m^{-2} and $\rho \approx 2.5$ m^{-2}.

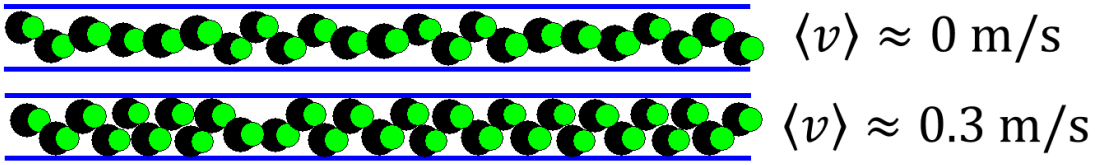

Figure 13: Pedestrians' spacial distribution in a corridor of $b_{cor} = 1$ m explaining the behaviour shown in Fig.12 for the MSFM. When $N = 23$, pedestrians align in such a way their respect region is always trespassed impeding motion. When $N = 30$, the disposition of pedestrians allow some of them to display unoccupied respect regions, thus pushing the others and allowing some motion.

The straight corridor has also been addressed experimentally in [23]. Empirical results

point out significant discrepancies with the predictions of the models. A smoother decay is shown from the very beginning, with no clear onset of motionless regime in the interval $\rho \leq 4$ m^{-2}.

3.2.2 Funneled corridor

Fig.14 shows a new geometry based on the previous corridor. Three parameters define the facility: the maximum width of the corridor b_{cor1}, the minimum width b_{cor2} and the length l_c. The measurement region is defined by m_d and is equally separated from the exit and the entrance. This kind of geometry is inspired by the results of evolutionary optimization of a bottleneck [28]. We wondered if a geometry that enhances the outflow of pedestrians would actually show the same fundamental diagram as the straight corridor.

The fundamental diagram has been investigated as a function of the length of the corridor l_c for fixed widths $b_{cor1} = 6$ m and $b_{cor2} = 2$ m. The set of lengths studied was $l_c = 10, 15, 20$ m in a measurement region delimited by $m_d = 3$ m. Note the angle of the escape route changes with l_c. Results are registered in Fig.15. Significant differences are found with respect to the straight corridor. In the SFM, a maximum in velocity is found at $\rho \approx 3.1$ m/s followed by a constant decay rate, apparently regardless the corridor length l_c. No motionless regime is found in the interval $\rho \leq 4$ m^{-2} The CSFM presents a slightly different behaviour than the SFM, characterized by a greater decay in the velocity from $\rho \approx 2.6$ m^{-2} on. No differences in the fundamental diagram with respect to l_c can be noted in the ASFM reaching immobility at $\rho = 2$ m^{-2}. In the MSFM, two decay regimes that finally find immobility at $\rho_0 = 3$ m^{-2} are found.

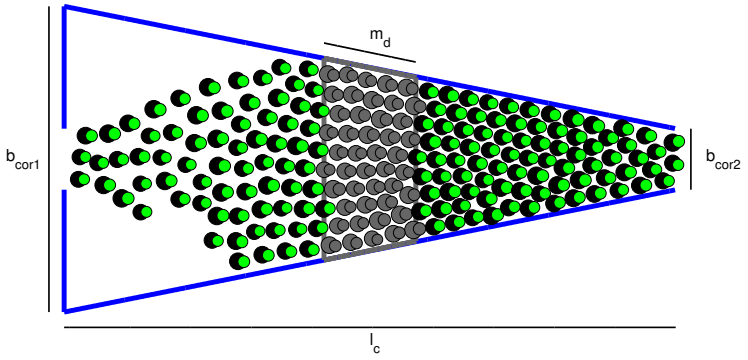

Figure 14: Geometry of the simulated funneled corridor for the measurement of the fundamental diagram. The snapshot corresponds to a simulation with $m_d = 3$ m, $l_c = 20$ m and $b_{cor1} = 2$ m and $b_{cor2} = 10$ m.

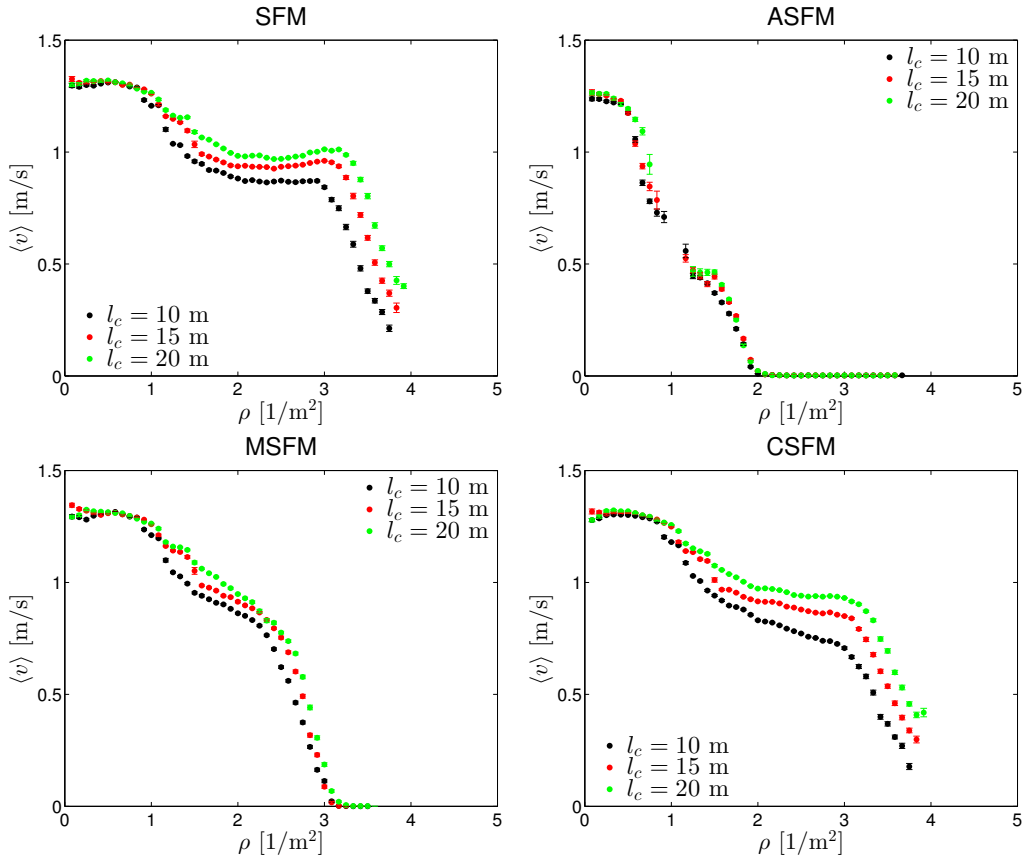

Figure 15: Fundamental diagrams of a funneled periodic corridor of $b_{cor1} = 6$ m and $b_{cor2} = 2$ as a function of the length l_c. Social Force Model (SFM), Anisotropic Social Force Model (ASFM), Modified Social Force Model (MSFM), Centrifugal-Inspired Social Force Model (CSFM).

3.2.3 Rectangle

Fig.16 shows a rectangular geometry consisting of two corridors of different lengths l_{c1}, l_{c2} and widths b_{cor1}, b_{cor2}. The measurement area is restricted by the distance m_d. Pedestrians were headed counterclockwise to the nearest point of the dashed lines.

The fundamental diagram was studied as a function of b_{cor2} for fixed $l_{c1} = 7$ m, $l_{c2} = 3$ m and $b_{cor1} = 3$ m. The set of widths studied was $b_{cor2} = 1, 2, 3, 4, 5$ m. The measurement region side was $m_d = 4$ m. Results are registered in Fig.17. Noticeable differences with respect to the previous configurations sets are found. A change in the curvature of the fundamental diagram is encountered in the SFM, MSFM and CSFM for different values of the parameter b_{cor2}. However, in all cases they find immobility at the same $\rho_0 \approx 4$ m^{-2}. The CSFM slightly modifies the results provided by the SFM by increasing the first decay rate. The ASFM presents similar results for the different widths of the corridor b_{cor2} except for $b_{cor2} = 1$ m. Inmobility is found at $\rho_0 = 2$ m, regardless the geometry. The MSFM predicts the motionless regime at $\rho_0 \approx 3$ m.

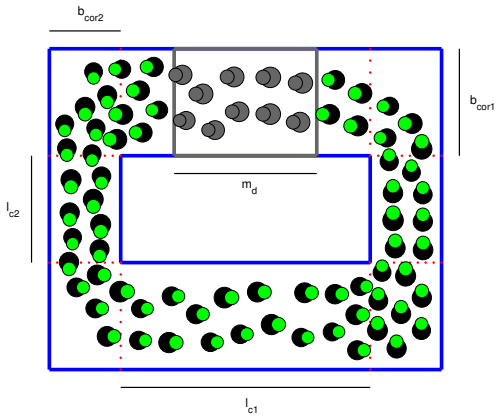

Figure 16: Geometry of the simulated rectangular facility for the measurement of the fundamental diagram. The snapshot corresponds to a simulation with $m_d = 4$ m, $l_{c1} = 7$ m, $b_{cor1} = 3$ m, $l_{c2} = 3$ m $b_{cor2} = 2$ m

.

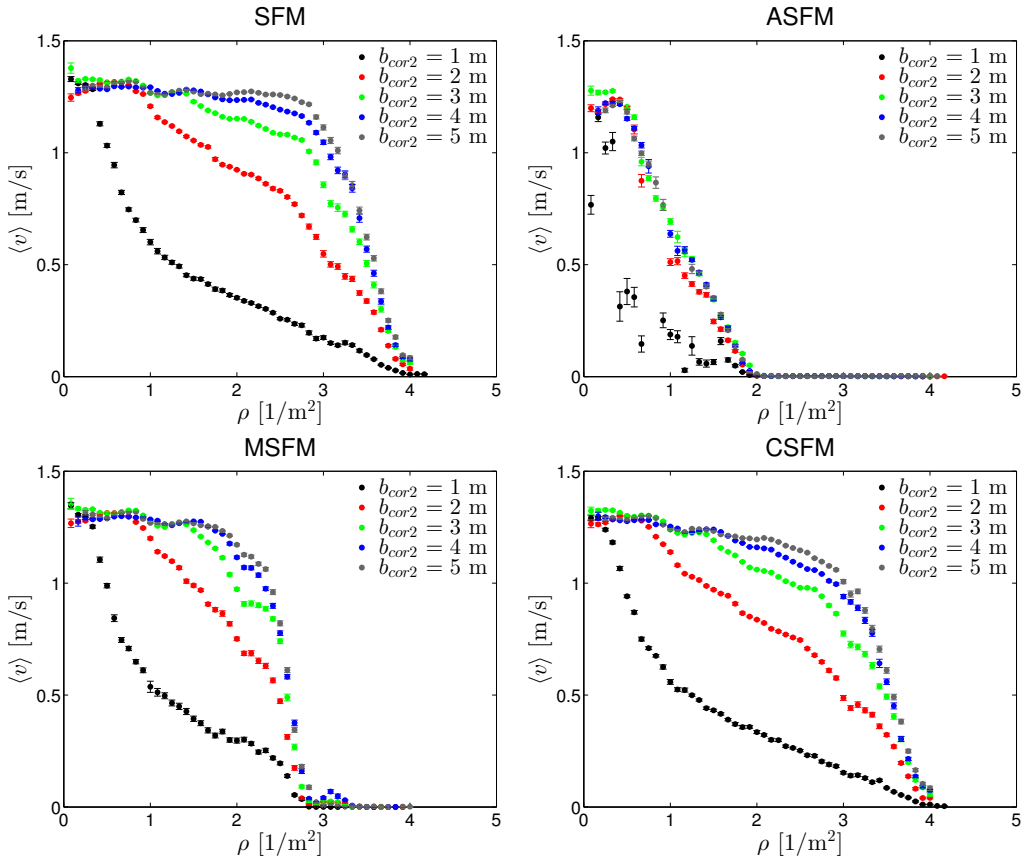

Figure 17: Fundamental diagrams of a rectangular facility of $l_{c1} = 7$ m, $b_{cor1} = 3$ m and $l_{c2} = 3$ m as a function of the width b_{cor2}. Social Force Model (SFM), Anisotropic Social Force Model (ASFM), Modified Social Force Model (MSFM), Centrifugal-Inspired Social Force Model (CSFM).

3.2.4 Racetrack

Fig.18 shows a racetrack scenario. The parameters that define the structure are the next: the width of the corridor b_{cor}, the distance between the two corridors d_{cors} and the length of the corridors l_c. The length of the measurement region is given by m_d. Pedestrians headed clockwise to the nearest point along the dashed lines. 10 different target locations were defined throughout the facility.

The fundamental diagram has been investigated as a function of the width of the corridor b_{cor} for fixed values $l_c = 9.92$ m and $d_{cors} = 3.18$ m. The set of widths studied was $b_{cor} = 1, 2, 3.5, 4$ m. The measurement region side was $m_d = 6$ m. Results are presented in Fig.19. The SFM and CSFM present no apparent differences in their predictions displaying both $\rho_0 \approx 4$ m^{-2}. The ASFM shows slightly different decay rates and $\rho_0 \approx 1.9$ m^{-2} depending on b_{cor}. Predictions by the MSFM include different ρ_0 depending on b_{cor}. The same anomalous behaviour already commented in the straight corridor is found here.

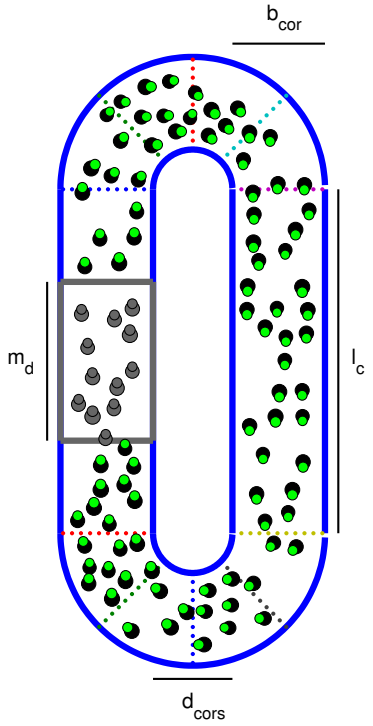

Figure 18: Geometry of the simulated racetrack for the measurement of the fundamental diagram. The snapshot corresponds to a simulation with $m_d = 6$ m, $l_c = 13$ m, $b_{cor} = 3.5$ m and $d_{cors} = 3$ m.

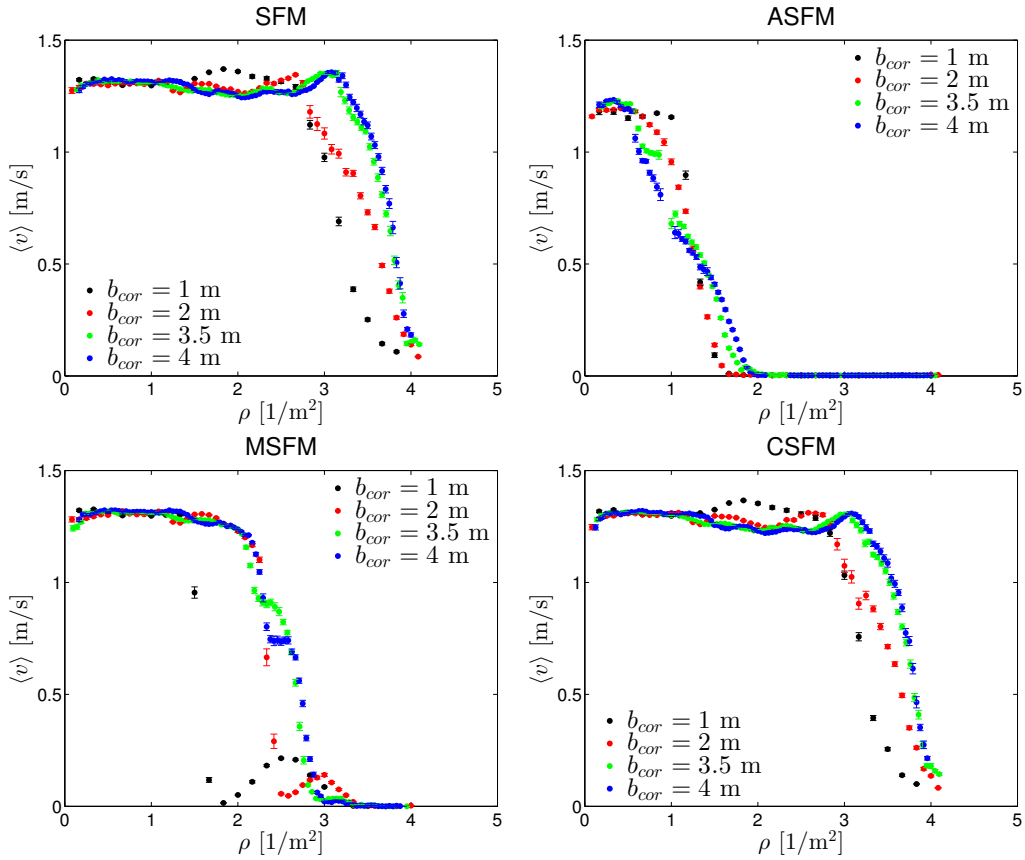

Figure 19: Fundamental diagrams of a racetrack of $l_c = 9.92$ m, $d_{cors} = 3.18$ m as a function of the width b_{cor}. Social Force Model (SFM), Anisotropic Social Force Model (ASFM), Modified Social Force Model (MSFM), Centrifugal-Inspired Social Force Model (CSFM).

Similar geometries have been addressed by means of both models and experiments [24, 29]. Clear discrepancies with the experimental data are met by the results of the models. A smoother decay rate is empirically found. In [24] discrepancies with respect to the MSFM at high densities are said to reduce if a normal distribution of respect factors is implemented. This allow some pedestrians with small respect regions to display them unoccupied even at high densities thus pushing the rest and generating some motion. Along the lines of the previous reasoning, the ASFM could soften the decay process by providing a normal distribution for λ. These two scenarios are studied in Fig.20. The decay rate of the MSFM presents a large dependency on the distribution of R_F in contrast to the ASFM.

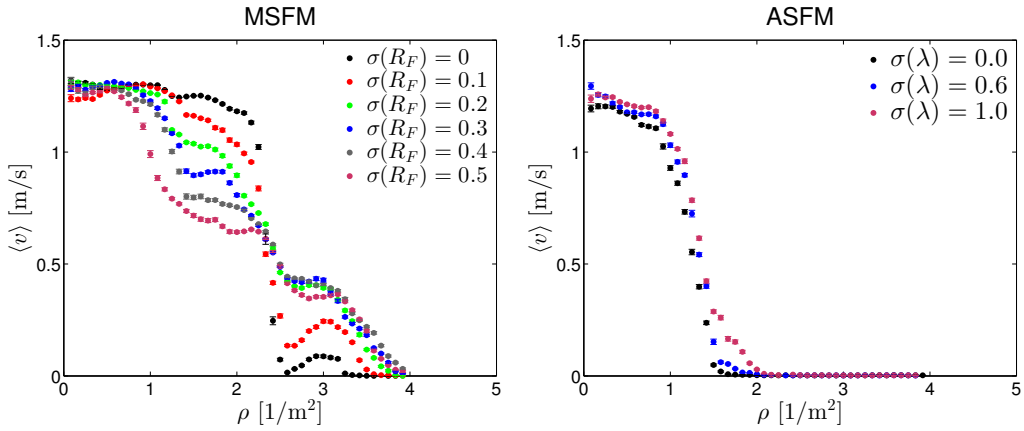

Figure 20: Behaviour of the fundamental diagram of MSFM and ASFM models in a racetrack configuration of $l_c = 7$ m, $d_{cors} = 1$ m and $b_{cor} = 2$ m when a gaussian distribution of R_F and λ were proposed. Since $R_F < 0$ and $\lambda < 0$ or $\lambda > 1$ lack of physical sense, whenever this values appeared they were rejected followed by a new proposal.

3.2.5 Circle

Fig.21 shows a circular shaped facility. It can be regarded as a special case of the racetrack geometry when $l_c = 0$ m. Two parameters define the structure: the inner and the outer radii, r_1 and r_2 respectively. The measurement region is defined by the angle α_{med}. Pedestrians' sense of motion is clockwise. The desired direction of motion is always tangent to the circumference centered in the center of the facility of radius the distance the pedestrian keeps from the center. If the reference system is set in the center of the facility: $\mathbf{e}_i^0(t) = (r_i(t)^2, -r_i(t)^1)/||\mathbf{r_i(t)}||$. Due to inertia effects, pedestrians tend to separate from the center as shown in Fig.21.

The fundamental diagram has been investigated as a function of one of the radii r_2 for a constant $r_1 = 1$ m. The set of radii studied were $r_2 = 2, 3, 4, 5, 6$ m in a region defined by an angle $\alpha_{med} = 90^o$. Results are registered in Fig.22. No differences are found between the SFM and the CSFM predictions. The noticeable differences as a function of r_2 in the predictions of the SFM and CSFM are greatly reduced in the ASFM and MSFM results. The motionless regime is found at $\rho_0 \approx 2$ m^{-2} and $\rho_0 \approx 3$ m^{-2} for the ASFM and MSFM respectively. Nevertheless, an important deviation is shown for $r_2 = 2$ m in the MSFM predictions.

Experimental measurements of pedestrians walking in line in a ring-shaped facility were taken in [30]. A smoother decay rate is found starting from $\rho \approx 0$ m^{-2}. Despite the different inner radius, these results would seem unlikely to be found by the models.

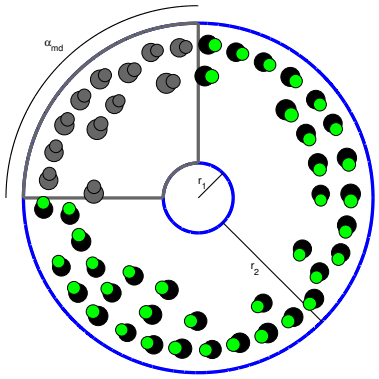

Figure 21: Geometry of the simulated circular facility for the measurement of the fundamental diagram. The snapshot corresponds to a simulation with $r_1 = 1$ m, $r_2 = 5$ m.

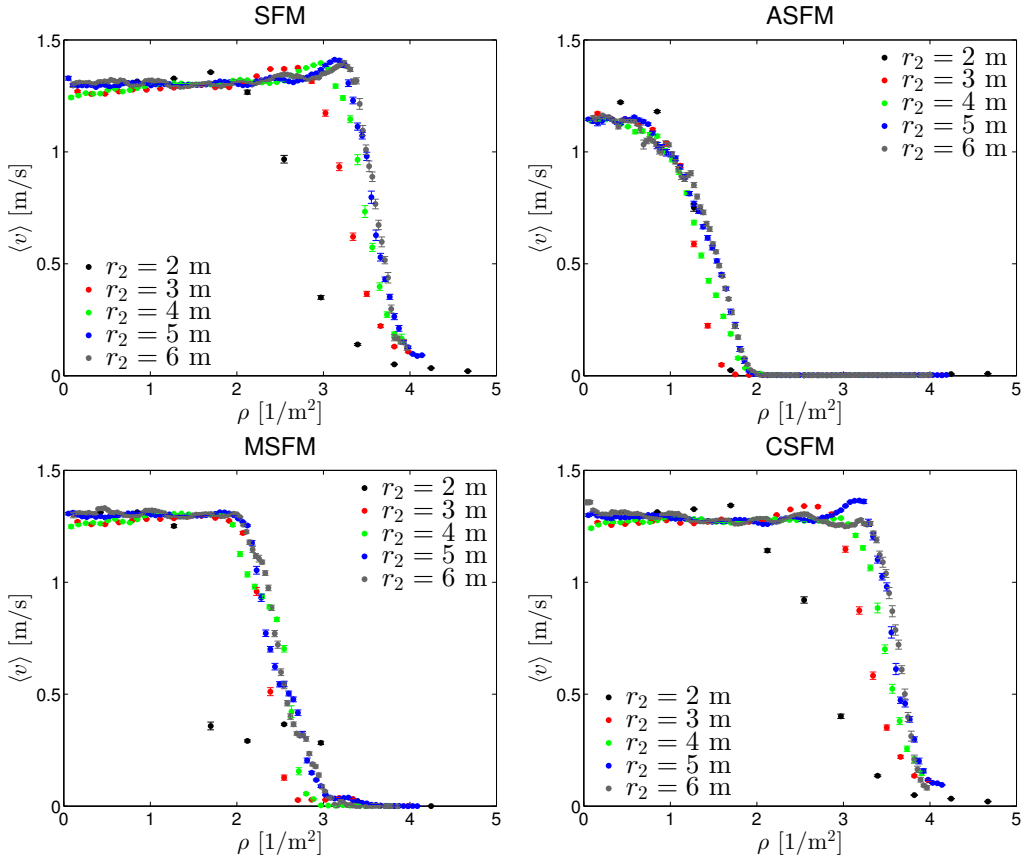

Figure 22: Fundamental diagrams of a circular facility of $r_1 = 1$ m as a function of the outer radius r_2. Social Force Model (SFM), Anisotropic Social Force Model (ASFM), Modified Social Force Model (MSFM), Centrifugal-Inspired Social Force Model (CSFM).

3.2.6 Bidirectional corridor

Fig.23 shows a straight corridor filled by pedestrians moving in the two senses of motion. The structure of the facility is defined by the width b_{cor} and the length l_c. The measurement region is the area in grey, characterized by the distance m_d.

The fundamental diagram was studied as a function of the width b_{cor} for a constant length $l_c = 15$ m and equal number of pedestrians of each group. The set of widths studied was $b_{cor} = 5, 6, 7$ m in a region defined by $m_d = 4$ m. Results are registered in Fig.24. The SFM predicts two different regimes. The CSFM acts lifting the velocities up to $\rho \approx 2$ m^{-2}, defining a unique rate of decay from $\rho \approx 1$ m^{-1} on. This is attributed to the fact that the CSFM prevents pedestrians from strong collisions to a greater extent than the SFM at small densities. Both models predict the onset of immobility at $\rho_0 \approx 2.9$ m^{-2}. The MSFM presents the same qualitative behaviour as the SFM but an earlier $\rho_0 \approx 2.5$ m^{-2} is predicted. The ASFM shows an initial rapid decay with an unpredicted behaviour for $b_{cor} = 7$ m. Deviations from the apparent trend of the curve in the previous models are probably due to the break of jams in the surroundings of the measurement area.

Experimental studies of bidireccional flows in corridors were studied in [31, 21]. Most remarkably, no clear onset of motionless regime is found in the interval $\rho \leq 4$ m^2. The variance in experimental measurements makes it hard to establish a clear trend to compare with the models.

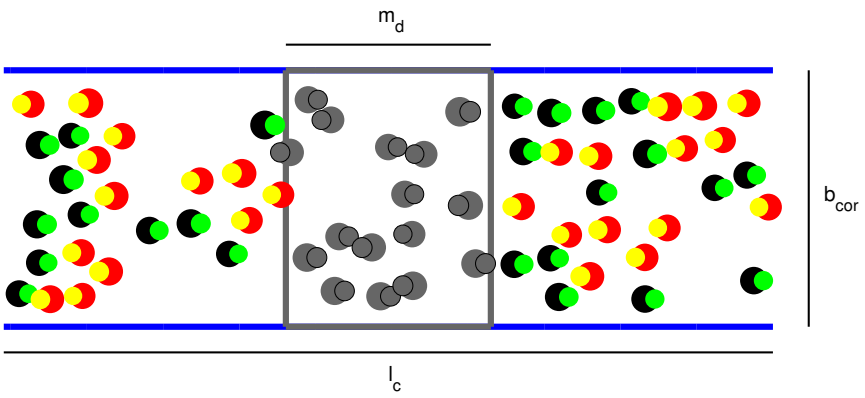

Figure 23: Geometry of the simulated bidireccional corridor for the measurement of the fundamental diagram. The snapshot corresponds to a simulation with $b_{cor} = 5$ m, $l_c = 15$ m and $m_d = 4$ m.

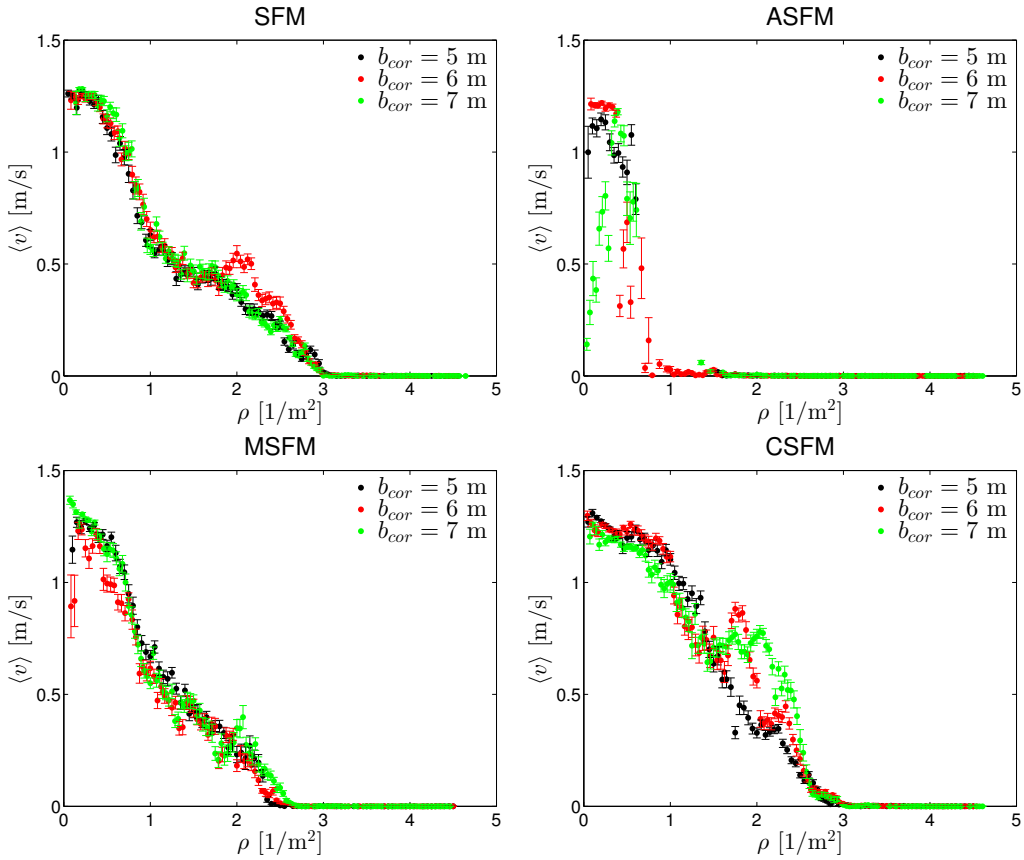

Figure 24: Fundamental diagrams of a bidireccional corridor facility of $l_c = 15$ m as a function of its width b_{cor}. Social Force Model (SFM), Anisotropic Social Force Model (ASFM), Modified Social Force Model (MSFM), Centrifugal-Inspired Social Force Model (CSFM).

3.2.7 Corridor intersection

Fig.25 shows the geometry of two intersecting perpendicular corridors. The structure is defined by the width of the two corridors involved b_{cor1}, and b_{cor2} and the length of the corridors l_c. The measurement region is the rectangular area shared by the two corridors. Two types of pedestrians are represented in the figure. Pedestrians in black steer along corridor 1 while pedestrians in red do it along corridor 2. Periodic boundary conditions have been set in the limits of the corridors. However, this periodicity only applies to pedestrians supposed to move in these corridors. Pedestrians in black experience periodic boundary conditions in corridor 1, but they do not display them when they reach the limits of corridor 2. The same occurs with pedestrians in red placed along the perpendicular corridor to their natural pace. When high densities are attained, pedestrians of one corridor can shift pedestrians of the other corridor to their natural corridor. This is a feature depicted in panic situations. It has been captured in Fig.25. Note that several pedestrians in black lie along corridor 2. When this is the case, pedestrians are headed to the common region and from then to their original target. Every time a pedestrian reaches the limit of the corridor in which it is not intended to move all the pedestrians are initialized again.

The fundamental diagram was studied as a function of the width of the second corridor b_{cor2} for a constant $b_{cor1} = 3$ m and equal number of pedestrians in each corridor. The set of widths studied was $b_{cor2} = 2, 3, 4$ m. A comparison between the predictions of the SFM, ASFM and CSFM as obtained so far and after introducing the effects of impatience was made. The effects of impatience in bidirectional flows are an increase in the desired velocity of motion and noise according to eq.8 and eq.9 respectively. The time considered for pedestrians to evaluate their level of panic was the previous $t_p = 5$ s. Only 80% of pedestrians were prone to get impatient. The rest did not modify their motion conditions under any circumstances. The maximum velocity attained due to panic was set a function of the original desired velocity as

$$v_i^{max} = (1.5 + 1.5 \cdot \hat{u}) \cdot v_i^0,$$

where $\hat{u}$ is a uniform random variable providing random numbers between 0 and 1. In order for pedestrians to display proportional levels of noise and velocity increments the maximum noise reachable was set dependent on the maximum velocity attainable as

$$\eta_i^{max} = \eta_i^0 + \frac{v_i^{max} - min(v_i^{max})}{max(v_i^{max}) - min(v_i^{max})} \cdot \eta^{max},$$

where $min(v_i^{max}) = 1.65$ m s^{-1} is the maximum velocity reachable by the slowest pedestrian, $max(v_i^{max}) = 4.5$ m s^{-1} is the maximum velocity attainable by the fastest pedestrian, $\eta_i^0 = 15$ and $\eta^{max} = 90$.

Results are presented in Fig.27. Non significant differences are found as a function of the width of the corridor b_{cor2}. Impatience in pedestrians has the effect of lifting slightly the fundamental diagram to higher values of velocity. Due to the tendency of the ASFM to generate jams, an additional series of 14 measurement simulations were performed in the low density regime in order for the fundamental diagram to display results bellow $\rho = 1$ m^{-2}, otherwise not found.

The intersection of corridors with two flows as studied here has been experimentally addressed in [32]. The experimental fundamental diagram present higher values of velocity, and once more, no onset of immobility in the interval $\rho \leq 4$ m^{-2}. However, differences in the conditions of the experiment should be taken into account if a detailed comparison was made.

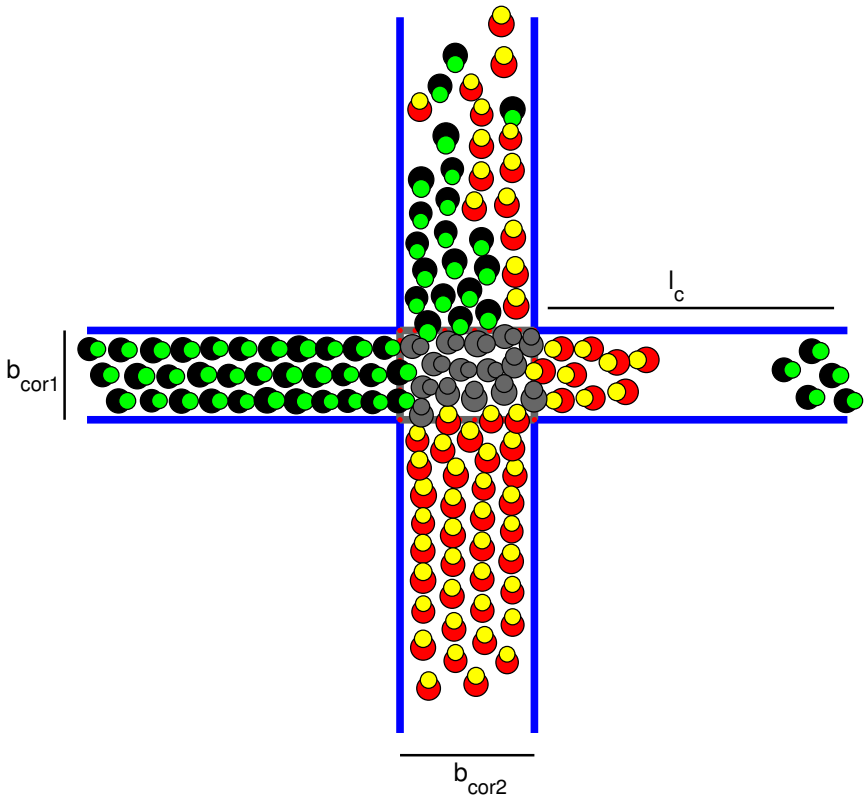

Figure 25: Geometry of the simulated intersection of straight corridors facility for the measurement of the fundamental diagram. The snapshot corresponds to a simulation with $b_{cor1} = 2$ m and $b_{cor2} = 3$ m and $l_c = 7$ m.

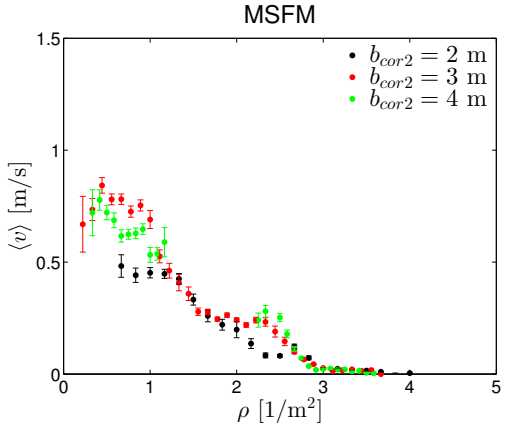

Figure 26: Fundamental diagram of an intersection of corridors of $l_c = 10$ m and $b_{cor1} = 3$ m as a function of b_{cor2} by means of the Modified Social Force Model (MSFM).

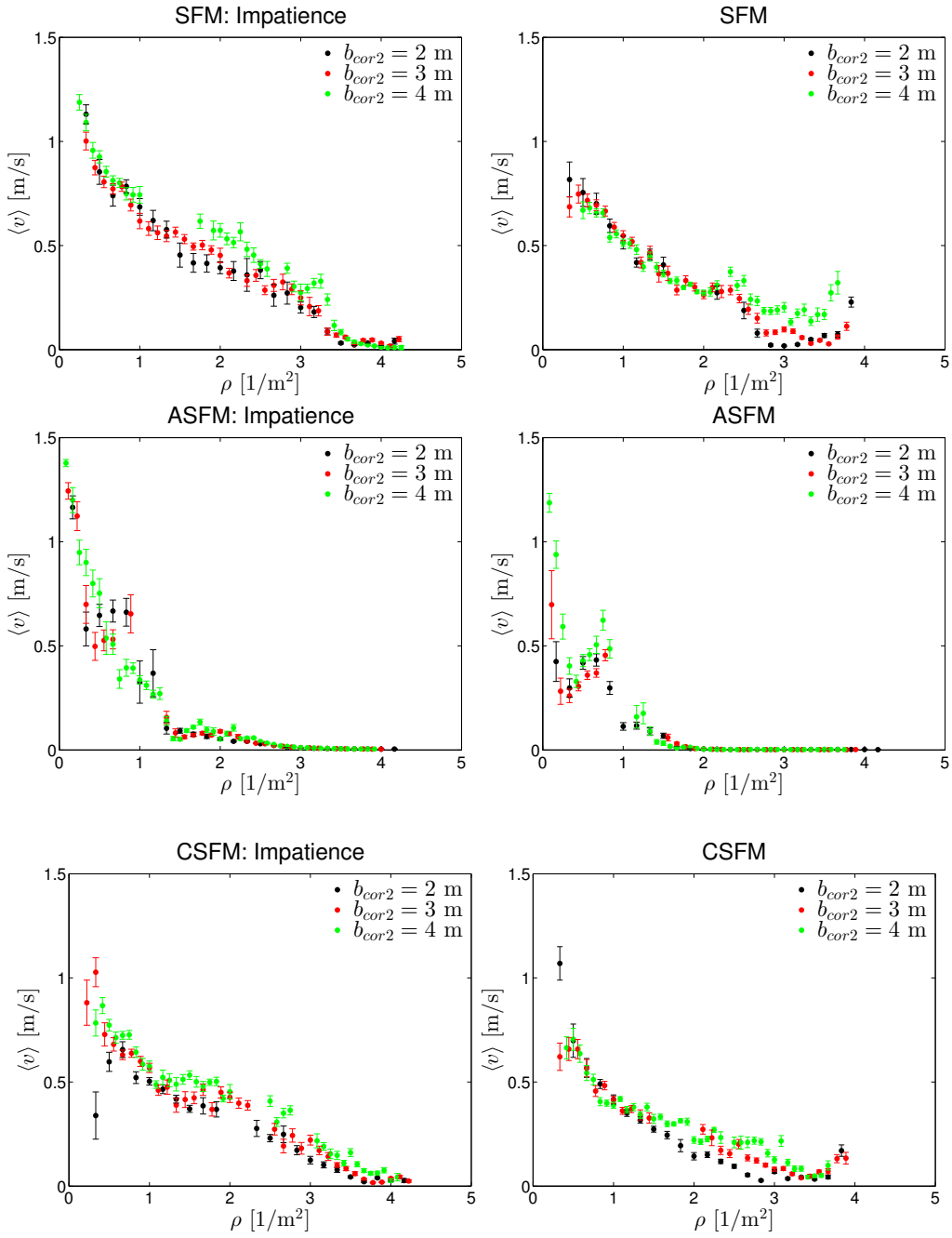

Figure 27: Fundamental diagrams of an intersection of corridors of $l_c = 10$ m and $b_{cor1} = 3$ m as a function of b_{cor2} with and without the introduction of impatience effects. Social Force Model (SFM), Anisotropic Social Force Model (ASFM), Modified Social Force Model (MSFM), Centrifugal-Inspired Social Force Model (CSFM).

4 Conclusions and future work

An investigation of the fundamental diagram predicted by the Social Force Model, Anisotropic Social Force Model, Modified Social Force Model and Centrifugal-Inspired Social Force Model as a function of the geometry has been conducted. The geometries evaluated with unidireccional flows were the straight corridor, the funneled corridor, a rectangular facility, a racetrack and a circular facility. The geometries analyzed in counterflows were the straight corridor and an intersection of corridors. In the last one, the effects of impatient and pushy pedestrians were studied. The fundamental diagram predicted by the social force models cannot be considered universal. Relevant differences are found depending on the geometry.

Regarding unidirectional flows, the ASFM ($\lambda = 0.1$) predicts more stable results than the other models. In a sense, the Anisotropic Social Force Model is the most fundamental of them. It predicts an onset of the motionless regime at $\rho_0 \approx 2$ m^{-2} regardless the geometry. The CSFM ($d^C = 2$ m, $C_i = 1$) presents no noticeable effects in the fundamental diagram with respect to the SFM in the straight corridor, the racetrack and circle. It acts dropping slightly the results encountered by the SFM in the remaining geometries. Its effects are probably undermined by the small range of desired velocities and masses set in the experiment. The MSFM ($R_F = 0.7$ m) predicts an onset immobility around $\rho_0 \approx 3$ m^{-2}. An anomalous behaviour was observed for certain geometries due to the configuration of pedestrians in space at different densities. This effect was disregarded in the original publication of this model modification and suggests important limitations to the model.

As far as counterflows are concerned, fluctuations in the fundamental diagram are attributed to the presence of jams in the surroundings of the measurement area. The ASFM presents a remarkable tendency to generate jams. The effects of impatient pedestrians facilitates motion by lifting the fundamental diagram. In order to minimize the unwanted effect of jams in the fundamental diagram, the length of the corridor must be largely increased.

Two mechanisms are proposed in order to make the measurement process more efficient. In this work walls were discretized in the space. The distance between a walker and all the point like walls was evaluated every time step. Then, only walls within a given distance were considered to interact. Instead, a different and unique point like wall could be computed for every pedestrian given its location in space without a previous pre-implementation. This would help save computational time, although this procedure would reduce the force effectuated by walls. If a large study of a facility as a function of its size where a large number of pedestrians is to be reached is conducted, the *link cell method* is proposed to reduce the computational complexity from $O(N^2)$ to $O(N)$, where N is the number of pedestrians.

A quick look at the experimental data in unidirectional flows let us see models do not match the smooth decay often registered empirically. However, the same exact calibration appears to be more appropriate in bidirectional flows. The onset of immobility is never met by the experimental results, which do not display it in the interval $\rho \leq 4$ m^{-2}. Regarding future work, a detailed comparison between models and experiments could

be made in order to unveil how the geometry actually affects the diagram and how the models adjust to the shape of the function. This would also allow to calibrate the studied models and/or suggest new modifications to account for the differences encountered.

References

[1] October 29, (2015), Death toll in Saudi haj disaster at least 2,070: Reuters tally. Retrieved August 1, 2017 from http://www.reuters.com.

[2] Helbing, D., Johansson, A. (2010). Pedestrian, Crowd and Evacuation Dynamics. *Encyclopedia of Complexity and Systems Science, 16*, 6476.

[3] Hankin, B. D., Wright, R. A. (1958). Passenger flow in subways, *Operational Research Quarterly, 9*, 81.

[4] Carrillo, J. A., Martin, S., Wolfram, M. T., A local version of the Hughes model for pedestrian flow, Arxiv e-print, arXiv:1501.07054.

[5] Helbing,D. (1992). A Fluid-Dynamic Model for the Movement of Pedestrians, *Complex Systems, 6*, 391.

[6] Helbing, D., Molnar, P. (1995). Social force model for pedestrian dynamics, *Physical Review E, 51*, 4282.

[7] Helbing, D., Farkas, I., Vicsek, T. (2000). Simulating dynamical features of escape panic, *Physical Review Letters, 84*, 1240.

[8] Steiner, A., Philipp, M., Schmid, A. (2007). Parameter Estimation for a Pedestrian Simulation Model, 7^{th} Swiss Transport Research Conference, Ascona.

[9] Johansson, A., Helbing, D., Shukla, P. K. (2007). Specification of the Social Force Pedestrian Model by Evolutionary Adjustment to Video Tracking Data, *Advances in Complex Systems, 10*, 271.

[10] Helbing, D. (1991). A mathematical model for the behaviour of pedestrians, *Behavioral Science, 36*, 298.

[11] Helbing, D. (1992). A mathematical model for behavioral changes by pair interactions, in Haag, G., Mueller, U., Troitzsch, K. G. (Eds.), *Economic Evolution and Demographic Change. Formal Models in Social Sciences*, 330, Berlin, Springer.

[12] Sikora, W., Malinowski, J., Kupczak, A. (2012). Model of skyscraper evacuation with the use of space symmetry and fluid dynamic approximation, *Lecture Notes in Computer Science, 7204*, 924.

[13] Parisi, D. R., Negri, P. A. (2014). Sequential evacuation strategy for multiple rooms toward the same means of egress, *Papers in physics, 6*, 2.

[14] Carstens, R. L., Ring, S. L. (1970). Pedestrian capacities of shelter entrances, *Traffic Engineering, 41*, 38.

[15] Polus, A., Joseph, J. L., Ushpiz, A. (1983). Pedestrian flow and level of service, *Journal of transportation engineering, 109*, 46.

[16] Flötteröd, G., Lämmel, G. (2015). Bidirectional pedestrian fundamental diagram, *Transportation Research Part B, 71*, 194.

[17] Helbing, D., Johansson, A., Al-Abideen, H. Z. (2007). The Dynamics of Crowd Disasters: An Empirical Study, *Physical Review Letters E, 75*, 046109.

[18] Fruin, J. J. (1987). *Pedestrian Planning and Design*, New York, NY: Metropolitan Association of Urban Designers and Environmental Planners.

[19] Chattaraj, U., Seyfried, A., Chakroborty, P. (2009). Comparison of pedestrian fundamental diagram across cultures, *Advances in Complex Systems, 12*, 393.

[20] Morrall, J. F., Ratnayake, L. L., Seneviratne, P. N. (1991). Comparison of CBD Pedestrian Characteristics in Canada and Sri Lanka, *Transportation Research Record, 1294*, 57.

[21] Zhang, J., Klingsch, W., Schadschneider, A., Seyfried, A. (2012). Ordering in bidirectional pedestrian flows and its influence on the fundamental diagram, *Journal of Statistical Mechanics: Theory and Experiment, 2012*, 02002.

[22] Kholshevnikov, V. V., Shields, T. J., Boyce, K. E., Samoshin, D. A. (2008). Recent Developments in Pedestrian Flow Theory and Research in Russia, *Fire Safety Journal, 43*, 108.

[23] Zhang, J., Klingsch, W., Schadschneider, A., Seyfried, A. (2011). Transitions in pedestrian fundamental diagrams of straight corridors and T-junctions, *Journal of Statistical Mechanics: Theory and Experiment, 2011*, 06004.

[24] Parisi, D. R., Gilman, M., Moldovan, H. (2009). A modification of the Social Force Model can reproduce experimental data of pedestrian flows in normal conditions, *Physica A, 388*, 3600.

[25] Chraibi, M., Seyfried, A., Schadschneider, A. (2010). Generalized centrifugal-force model for pedestrian dynamics, *Physical Review E, 82*, 046111.

[26] Dridi, M. H. (2015). Simulation of High Density Pedestrian Flow: A Microscopic Model, *Open Journal of Modelling and Simulation, 03*, 81.

[27] Yu, W. J., Chen, R., Dong, L. Y., Dai, S. Q. (2005). Centrifugal force model for pedestrian dynamics, *Physical Review E, 72*, 026112.

[28] Helbing, D., Farkas, I., Molnar, P., Vicsek, T. (2002). Simulation of pedestrian crowds in normal and evacuation situations, *Pedestrian and evacuation dynamics, 21*, 21.

[29] Mori, M., Tsukaguchi, H. (1987). A new method for evaluation of level of service in pedestrian facilities, *Transportation Research Part 21 A, 3*, 223234.

[30] Jelić, A., Appert-Rolland, C., Lemercier, S., Pettré, J. (2012). Properties of pedestrians walking in line: Fundamental diagrams. *Physical Review E, 85*, 036111.

[31] Liu, X., Song, W., Lv, W. (2014). Empirical Data for Pedestrian Counterflow through Bottlenecks in the Channel, *Transportation Research Procedia, 2*, 34.

[32] Cao, S., Seyfried, A., Zhang, J., Holl, S., Song, W. (2017). Fundamental diagrams for multidirectional pedestrian flows. *Journal of Statistical Mechanics: Theory and Experiment, 2017*, 033404.